Karlsruhe Institute of Technology

Water concentration and swelling stresses at silica surfaces derived from literature data

- Estimation of mass-transfer coefficients

Theo Fett, Günter Schell

KIT SCIENTIFIC WORKING PAPERS 94

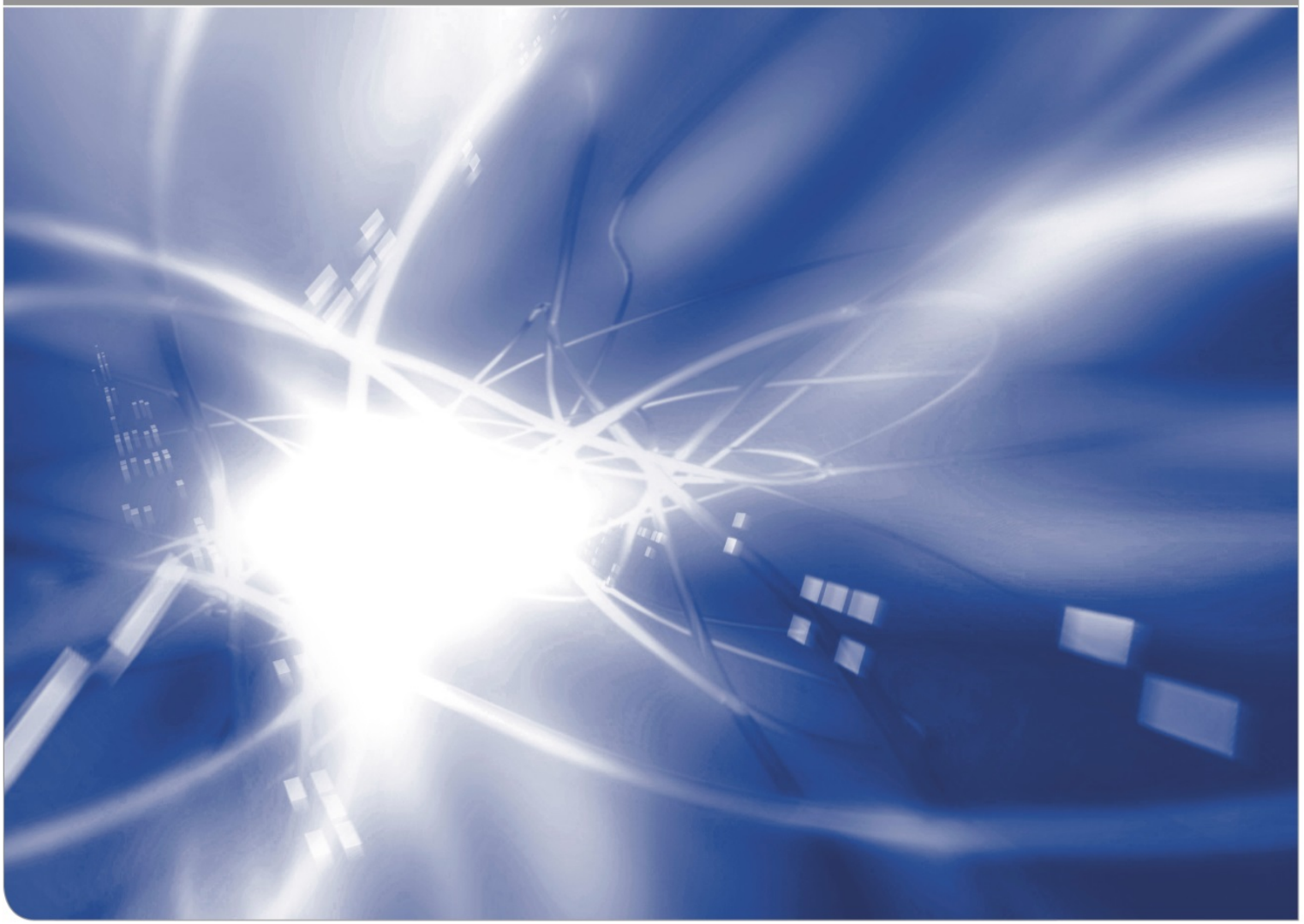

Institut für Angewandte Materialien, Karlsruher Institut für Technologie (KIT)

Impressum

Karlsruher Institut für Technologie (KIT)
www.kit.edu

2018

ISSN: 2194-1629

Abstract

Monotonously increasing water concentrations at silica surfaces can be described by a mass transfer surface condition for diffusion that hinders free water penetration from a water vapour environment into silica. So far, the related mass transfer coefficient has been determined predominantly for tests at temperatures ≥250°C. For an extension of the database, experimental results from literature at temperatures ≤ 200°C are studied. These measurements are surface water concentrations and disk curvature measurements, both under saturation vapour pressure.

Contents

1. Results by Helmich and Rauch [1]

1.1 Water concentrations

An extensive study on the uptake of water at silica surfaces was published by Helmich and Rauch [1]. In the present report we use these results obtained in vapour at saturation pressure in order to determine the water concentrations at the glass surface as a function of soaking time. Helmich and Rauch [1] used the NRA-Technique (Nuclear Reaction Analysis) for the determination of the hydrogen- and the oxygen concentration. In order to distinguish between water oxygen and the oxygen in the SiO_2 structure, they used water with ^{18}O content. For the H-concentrations in [1] a rather large scatter has to be taken into consideration as is visible from Fig. 1a for measurements at 200°C.

A fitting procedure according to the erfc-profile for the hydrogen concentration

$$H = H_{x=0}\,\mathrm{erfc}\left(\frac{x}{2\sqrt{Dt}}\right) \qquad (1)$$

(t=soaking time) resulted in the surface concentration $H_{x=0}$ and the diffusivity D. Figure 1b shows the surface H-concentrations vs. $\sqrt{t}$. Saturation is visible for $t \geq 144$h. The bars indicate the 90% Confidence Intervals (CI).

The results for $H_{x=0}$ are also compiled in Table 1 (last column) with the 90%-CI in brackets. Measurements on oxygen concentration showed negligible scatter. The ^{18}O surface concentrations are given in the third column of Table 1 and in Fig. 2a.

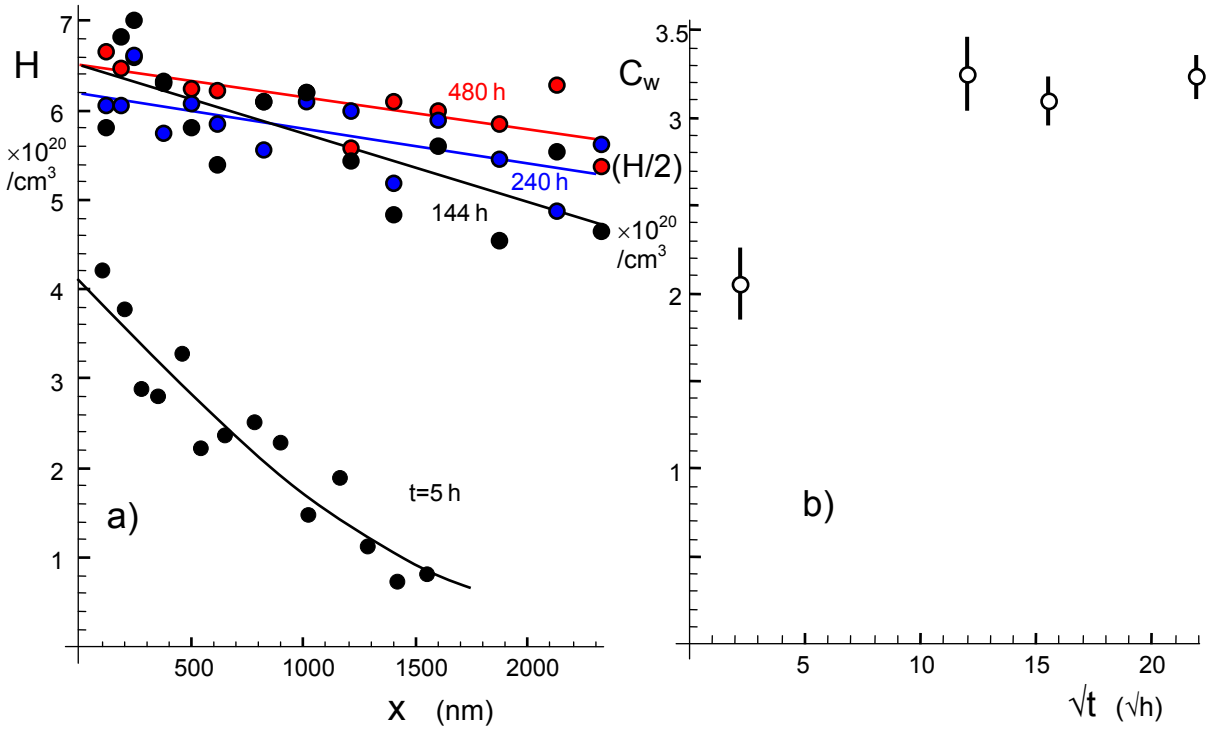

Fig. 1 a) Hydrogen concentration in the glass vs. depth x under the surface; b) related water concentrations at the surface with 90% Confidence Intervals.

For large times, $t \geq 144$h, the constant H-concentration indicates a constant water concentration at the surface, Fig. 2a. Nevertheless, the oxygen surface concentration increases continuously. The ^{18}O measurements are given by the solid circles and the result from the H-measurements as the open circles. The difference in the water contents from O- and H- measurements ΔC, Fig. 2b, must be caused by oxygen exchange in the O-data (exchange of ^{16}O of SiO_2 by the ^{18}O of the water). For discussion of the oxygen exchange see [1] and [2]. The difference ΔC is nearly proportional with time. This fact enables to transform the oxygen concentrations in water concentrations.
Figure 3 and the fourth column in Table 1 represent the corrected data. Again the water concentrations C_w from H/2 are plotted as the open symbols and those from oxygen measurements as the solid ones.

Temp. °C	Time h	From ^{18}O (10^{20})	O exchange eliminated	From H (10^{20}/cm^3)
200	5	2.12	2.04	4.11[3.71,4.51]
200	10	2.68	2.52	
200	20	3.19	2.86	
200	144	6.0		6.50[6.07,6.93]
200	240	8.0		6.20[5.92,6.48]
200	480	11.3		6.47[6.23,6.71]

Table 1 Results of water concentration from Helmich/Rauch [1].

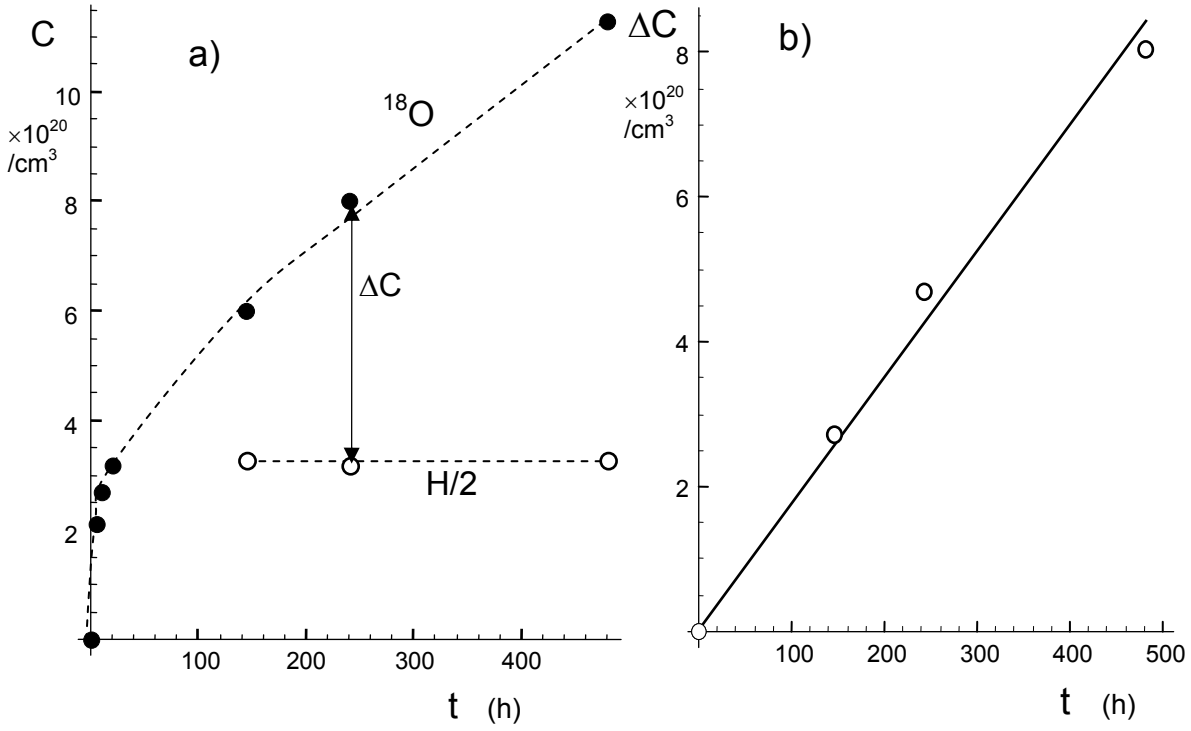

Fig 2 a) Results on oxygen surface concentrations from Helmich/Rauch [1] (solid circles), compared with the water concentration via hydrogen measurements (open circles), b) effect of oxygen exchange.

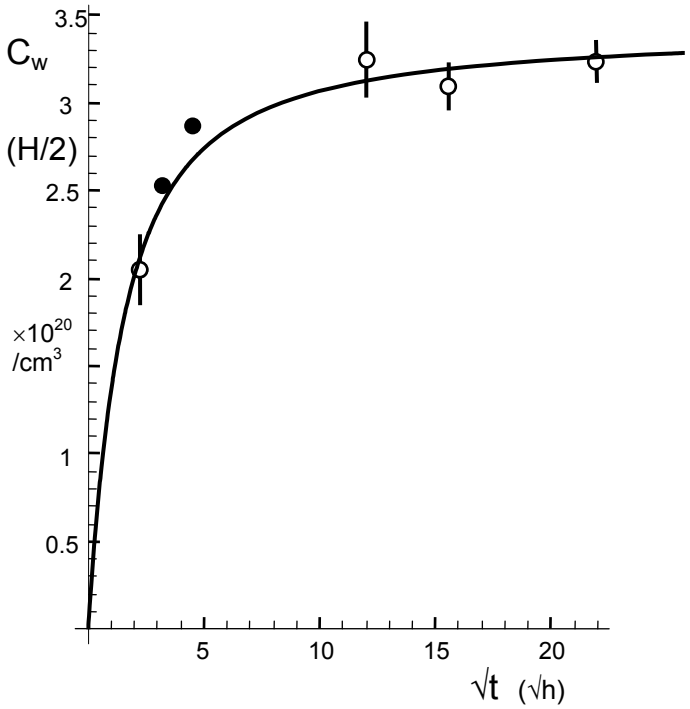

Fig. 3 Data from Fig. 1b compared with the oxygen results ($^{18}O/^{16}O$-exchange eliminated), (solid circles). The oxygen result at t=5h is identical with the value H/2 and therefore not visible.

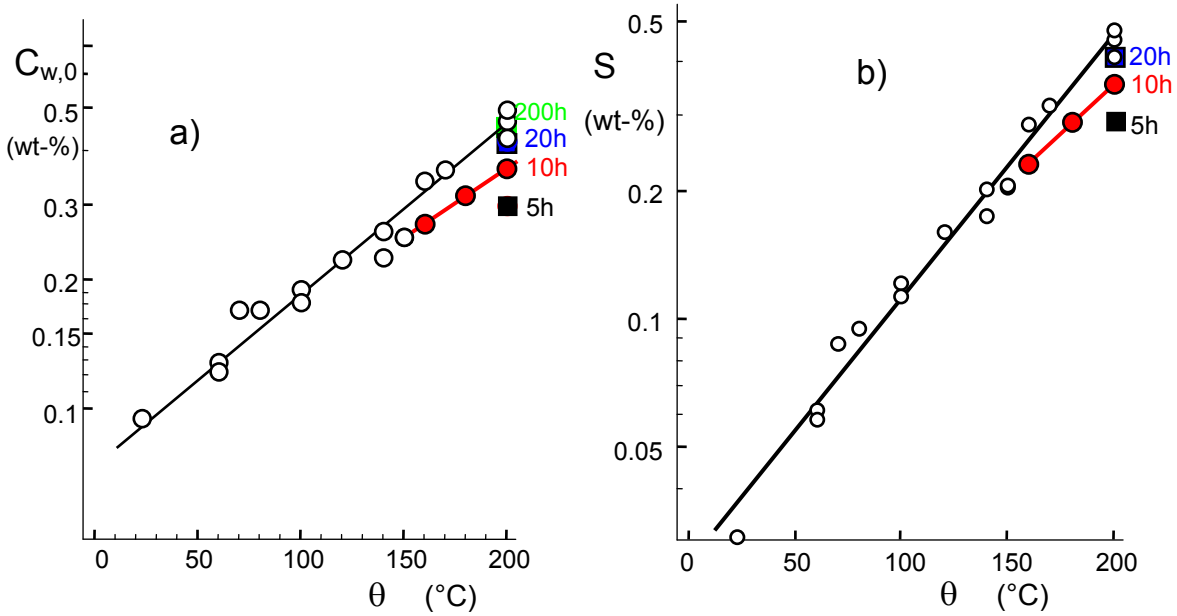

Fig. 4 a) Solubility of water at silica surfaces under saturation pressure by Zouine et al. [3] (open circles) and Helmich and Rauch [1] (red circles and squares); b) hydroxyl water species (same symbols as in part a)).

In *molar units*, the total water concentration is given by

$$C_w = C + \tfrac{1}{2}S = C(1 + \tfrac{1}{2}k) \qquad (2)$$

where the quantity k is the equilibrium constant describing the ratio of k=S/C.
The experimental results on equilibrium ratios from literature were expressed in [4] for the temperature range of 90°C≤T≤350°C by the empirical relation

$$k = \frac{S}{C} = A \exp\left(-\frac{Q}{RT}\right) \tag{3}$$

(A=32.3 and Q=10.75 kJ/mol). Equations (2) and (3) result in

$$C = \frac{C_w}{1+\frac{1}{2}k}, \quad S = \frac{C_w}{\left(\frac{1}{2}+\frac{1}{k}\right)} \tag{4}$$

and in *mass units*

$$S = \frac{17}{18}\frac{C_w}{\left(\frac{1}{2}+\frac{1}{k}\right)} \tag{5}$$

(the ratio 17/18 reflects the different mole masses of water and hydroxyl).

Temp. °C	Time h	C_w (wt-%)	S (wt-%)
200	5	0.299	0.289
200	10	0.367	0.355
200	20	0.421	0.408
200	200	0.439	0.425
180	10	0.316	0.305
160	10	0.272	0.244

Table 2 Results of total and hydroxyl water for interpolations with respect to temperature and time.

1.2 Analytical description of the time dependences via mass transfer coefficient

The data for $t \leq 20$h, which had to be corrected only slightly, were fitted as the total water concentration at the surface, C(0), according to

$$C(0) = C_\infty(1 - \exp[\alpha^2 t]\mathrm{erfc}[\alpha\sqrt{t}]) \tag{6}$$

with the mass transfer parameter abbreviated as

$$\alpha = \frac{h}{\sqrt{D}} \tag{7}$$

(h=mass transfer coefficient, D=Diffusivity). It has to be emphasized that eq.(6) is an approximation ignoring stress effects on diffusivity and solubility.

Curve fitting of eq.(6) to the results in Fig. 3 results in

$$\alpha = 0.523\ [0.468, 0.576](1/\sqrt{\mathrm{h}}),\ C_\infty = 3.48\,[3.40, 3.56]\times 10^{20}(\mathrm{H_2O/cm^3}) \tag{8}$$

(with the 90% confidence intervals in brackets). Equation (6) with the fitting parameters α and C_∞ of (8) is represented by the curve in Fig. 3. The value C_∞ is in agreement with the data by Zouine et al. [3] that were found in the range of 3.15-3.65×10^{20} (H_2O/cm^2).

2. Disk-soaking results by Wiederhorn et al. [4]

2.1 Bending moments and surface stresses

A second method to show the effect of water concentration on time has been shown by Wiederhorn et al. [4]. Stresses due to water in the surface region of silica were derived by measuring the change of the curvature of silica disks after hot-water soaking at 200°C. The bare silica disks were heat-treated on both sides and then stepwise etched from one side in a buffered HF solution. After each etching step the change of curvature was determined resulting in the released bending moment per unit width versus total removed surface layer as plotted in Fig. 5a for different soaking times.

The bending moment per unit width caused by a thin surface layer of stresses σ in a plate of thickness *W* is given by

$$M_b = \frac{W}{2} \times \int_0^W \sigma(z)\, dz \tag{9}$$

If the surface is removed by an amount of *d*, the remaining moment after a total surface removal (single etching depths accumulated) is

$$M_b(d) = \frac{W}{2} \int_d^W \sigma(z)\, dz \tag{10}$$

and the related change of moment

$$\Delta M_b(d) = \frac{W}{2} \int_0^d \sigma(z)\, dz \tag{11}$$

The left-hand side of (11) is known from measurements of curvature.

Equation (11) is an integral equation with respect to the unknown stress distribution σ(*z*). Since the integrand does not depend on *d* explicitly, its solution can simply be obtained by taking the derivative with respect to the removed layer thickness *d*

$$\sigma\big|_{z=d} = \frac{2}{W} \frac{\partial \Delta M_b}{\partial d} \tag{12}$$

This equation holds for the case that the removed layer-thickness is small compared with the thickness of the disk, i.e. for $d \ll W$.

The measured change of the bending moment per unit width (Nm/m) is plotted in Fig. 5a. In the procedure described in [4] the swelling stresses were first represented by appropriate erfc-type functions with unknown parameters and then integrated according to eq.(8), for details see [4]. The resulting bending moments were then fitted to the measured data resulting in the best set of parameters for the stress distribution σ(*z*). Figure 5b shows the stress distributions from [4]. Finally, Fig. 5c represents the stresses at the surface as a function of soaking time. The stresses slightly increase with time. The standard deviations for each of the measurements were for all tests with soaking times ≥20h maximum SD≤ 0.00037 Nm/m. Only for the short time of 2h at

196°C, a clearly larger standard deviation of about SD=0.001 Nm/m was found that was caused by warping of the disk. The red bars in Fig. 5a represent the spans of ±1 SD for the 196°C tests, which are in the case of the 20h soaking hardly visible.

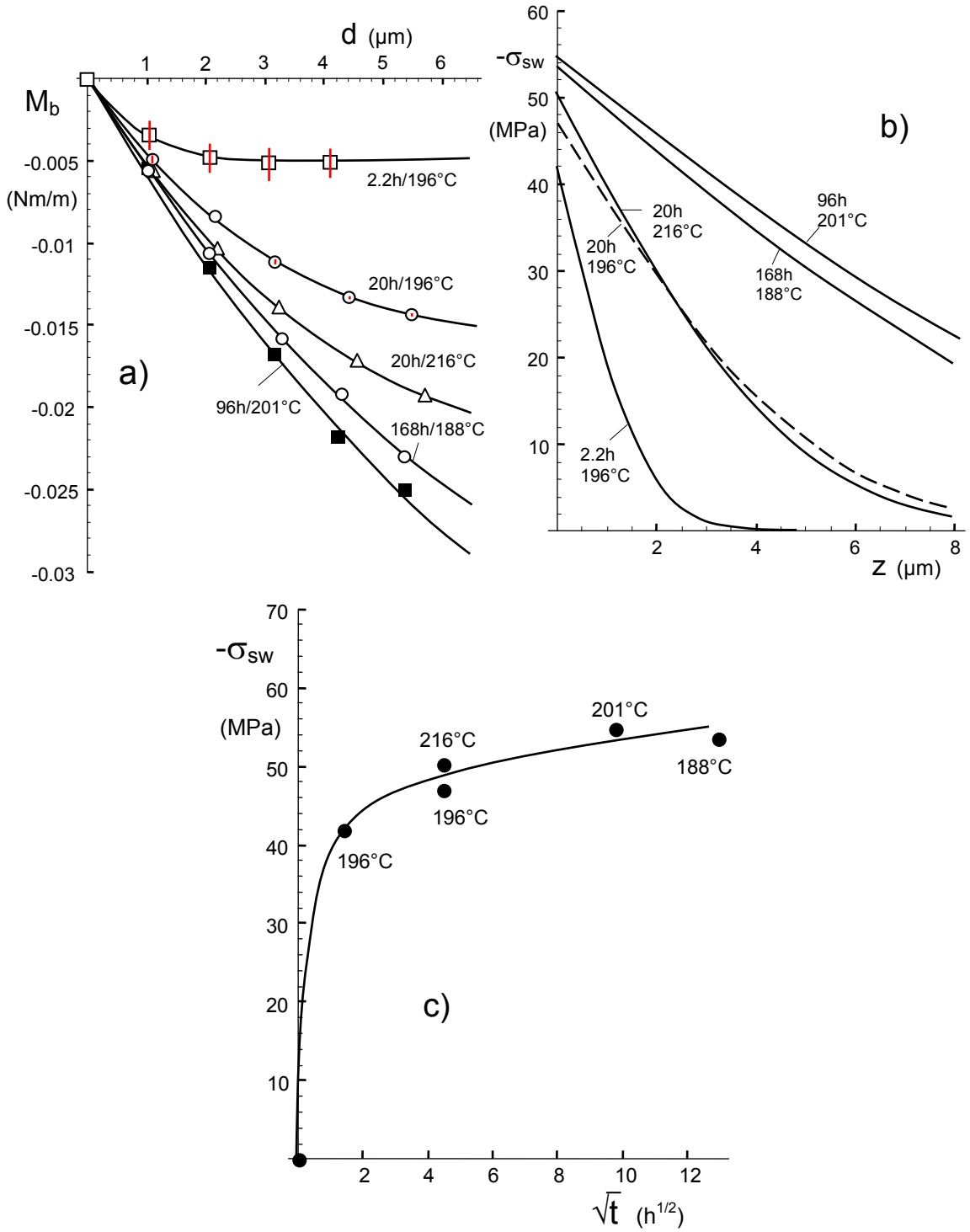

Fig. 5 a) Change of the bending moment during stepwise etching one surface (red bars for the 196°C tests represent ±1 SD), b) swelling stresses vs. depth, c) surface stresses as a function of time, data from [4].

2.2 Extended evaluation of results from [4]

As mentioned before, the results for disks soaked for 2.2h, Fig. 6a, the maximum standard deviations for the tests with $t \geq 20$h were at least 3-4 times smaller. Therefore, the rather large scatter for the tests with 2.2h soaking time may be addressed.

Figure 6 shows the individual results of the moment measurements as the circles measured at four angles on the disk. Whereas three of the moments showed the same standard deviation as all the other disks, at one angle the measurements are clearly different indicating warping of the disk. We repeated the evaluation in [4], represented by the squares, and tentatively excluded the deviating data. The result of the analysis is represented by the solid line in Fig. 6.

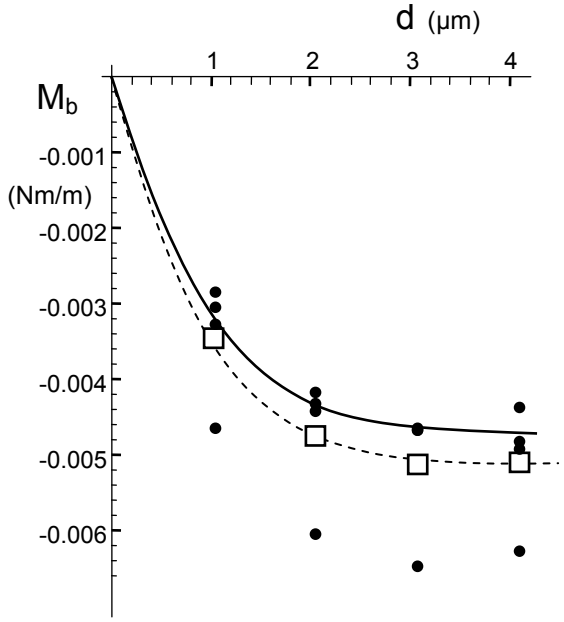

Fig. 6 Re-evaluation of 2h tests, individual moments (circles) compared with the data from Fig. 5a (squares); solid line: mean-value curve for the clearly deviating data points excluded.

Temperature/ Exposure Time (θ / t)	Measured surface stress [4] (MPa)	Surface stress for θ=200°C (MPa)
196 °C/2.2h	-41.8	-36.
196 °C/20h	-46.9	-48.6
216 °C/20h	-50.3	-43.4
201 °C/96h	-54.7	-54.2
188 °C/168h	-53.5	-59.8

Table 3: Prediction of surface stresses using mass transfer parameter $h/\sqrt{t}$, by eqs.(6, 7).

The determination of the saturation stress value for infinitely long times, σ_0, is of course hardly possible from Fig. 5c, because the apparent data "scatter" due to slightly different soaking temperatures is in the same order of magnitude as the expected further increase.

In this report we will first determine the saturation stress σ_0, the surface stress for long times, $t\to\infty$, when transient effects by a finite mass-transfer coefficient on surface concentrations are finished.

In context with the results of Table 1, we have to keep in mind that not a constant temperature of 200°C was involved in the tests. The soaking temperatures reached from 180°C to 216°C being responsible at least for a part of data "scatter".

The surface stress must be a function of time t and temperature θ. The first, t, is due to the restricted mass transfer from the environment into the surface that is time dependent, eq.(2). The latter is due to the temperature dependence of the water concentration C_0 that would be reached under saturation conditions and the temperature dependence of the mass-transfer parameter $h/\sqrt{D}$.

In order to eliminate the temperature dependence, we computed the ratio $S(\theta)/S(200°C)$ and corrected the systematic influence of deviating temperatures according to Table 2 by

$$\sigma(200°C) \cong \frac{S(200°C)}{S(\theta)}\sigma(\theta) \tag{13}$$

The results are entered in the last column of Table 3 and shown in Fig. 7a.

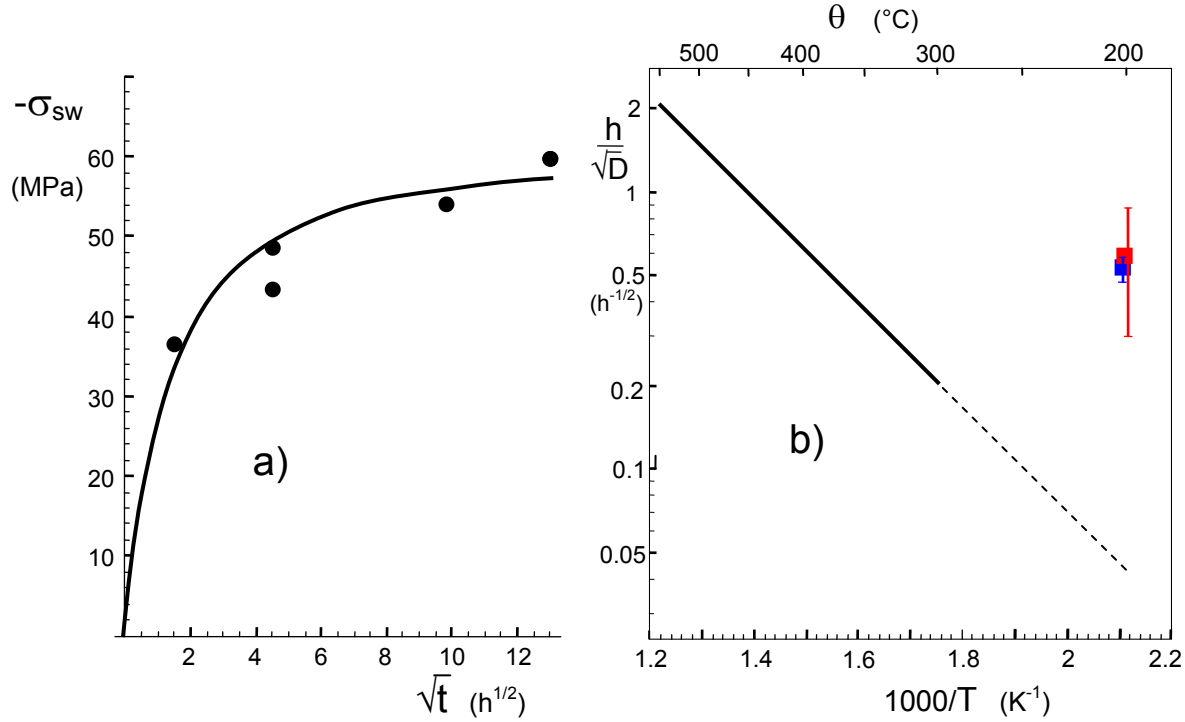

Fig. 7 a) Surface stresses for θ=200°C compared with the solid line according to eq.(14), dashed line as prediction for 200°C, b) parameter $h/\sqrt{D}$ as a function of temperature from [5], solid line. Symbols: $h/\sqrt{D}$ from eq.(8), blue square, and from eq.(15), red square. The vertical bars represent 90%-confidence intervals.

Since the swelling stresses are proportional to the hydroxyl concentration, $\sigma\propto S$, the mass transfer coefficient can be determined via

$$\sigma \cong \sigma_0(1-\exp[\alpha^2 t]\mathrm{erfc}[\alpha\sqrt{t}]) \tag{14}$$

by making the same assumption of negligible stress effects as mentioned in Section 1.2. Curve fitting of eq.(14) to the results in Fig. 7a yields the data

$$\alpha = 0.59\ (1/\sqrt{\mathrm{h}})\,[0.3,0.88]\,,\ \sigma_0 = -62\ \mathrm{MPa}\ [56;68] \tag{15}$$

Water uptake measurements were used in [5] to determine the parameter $h/\sqrt{D}$ in eq.(6). The parameters $h/\sqrt{D}$ could be described for temperatures ≥300°C (straight line in Fig. 7b) by

$$\frac{h}{\sqrt{D}} = A\,\exp\left(-\frac{Q}{RT}\right) \tag{16}$$

where the parameters were found to be $\log(A)$=5.82 -for A in $(1/\mathrm{h}^{1/2})$- and Q=35.1 (kJ/mol).

The result from eq.(8) is introduced in Fig. 7b by the blue square and the blue bar as the 90% confidence interval. The red square and bar show the result of eq.(15). These mass transfer parameters are by a factor of about 10 larger than expected from the extrapolated dependency, eq.(16), indicated by the dashed line. This strong increase will be discussed in a separate paper in the light of the results by Zhuravlev [6].

References

1 Helmich, Rauch, Glastech. Ber. **66**(1993), 195.

2 R.H. Doremus, Diffusion of Reactive Molecules in Solids and Melts, Wiley, 2002, New York.

3 A. Zouine, O. Dersch, G. Walter and F. Rauch, "Diffusivity and solubility of water in silica glass in the temperature range 23-200°C," *Phys. Chem. Glass: Eur. J. Glass Sci and Tech. Pt. B*, **48** [2] 85-91 (2007).

4 S. M. Wiederhorn, F. Yi, D. LaVan, T. Fett, M.J. Hoffmann, Volume Expansion caused by Water Penetration into Silica Glass, J. Am. Ceram. Soc. **98** (2015), 78-87.

5 S.M. Wiederhorn, G. Rizzi, S. Wagner, M.J. Hoffmann, T. Fett, Diffusion of water in silica glass in the absence of stresses, J. Am. Ceram. Soc. **100** (2017), 3895–3902.

6 L.T. Zhuravlev, The surface chemistry of amorphous silica. Zhuravlev model, *Colloids and Surfaces, A: Physicochemical and Engineering Aspects* **173**(2000), 1-38.

KIT Scientific Working Papers
ISSN 2194-1629

www.kit.edu